Visibility of Young's Interference Fringes: Scattered Light from Small Ion Crystals

Sebastian Wolf,[1,*] Julian Wechs,[2] Joachim von Zanthier,[2,3] and Ferdinand Schmidt-Kaler[1]
[1]QUANTUM, Institut für Physik, Universität Mainz, Staudingerweg 7, 55128 Mainz, Germany[†]
[2]Institut für Optik, Information und Photonik, Universität Erlangen-Nürnberg, Staudtstraße 1, 91058 Erlangen, Germany
[3]Erlangen Graduate School in Advanced Optical Technologies (SAOT), Paul-Gordan-Straße 6, Universität Erlangen-Nürnberg, 91052 Erlangen, Germany
(Received 3 December 2015; published 2 May 2016)

We observe interference in the light scattered from trapped $^{40}Ca^{+}$ ion crystals. By varying the intensity of the excitation laser, we study the influence of elastic and inelastic scattering on the visibility of the fringe pattern and discriminate its effect from that of the ion temperature and wave-packet localization. In this way we determine the complex degree of coherence and the mutual coherence of light fields produced by individual atoms. We obtain interference fringes from crystals consisting of two, three, and four ions in a harmonic trap. Control of the trapping potential allows for the adjustment of the interatomic distances and thus the formation of linear arrays of atoms serving as a regular grating of microscopic scatterers.

DOI: 10.1103/PhysRevLett.116.183002

The seminal double slit experiment by Young [1] is one of the most prominent experiments in physics. Originally, it formed the basis for understanding that light is a wave giving rise to phenomena like interference and diffraction, whereas in its modern interpretation it displays in a compact form the notion of wave-particle duality [2].

The original Young experiment employed transversally coherent light using a small aperture placed in front of the light source (in fact the Sun [1]). This results in electromagnetic waves at the two slits oscillating in phase and a visibility of the fringe pattern ~100%. The use of laser-driven atoms as "slits" enables the formation of more complex light fields, ranging from fully coherent to partially coherent and even fully incoherent fields. This transition arises from the fundamental process of photon scattering by the atoms. In the quantum theory of light [3–5] the scattering event involves the destruction of an incoming photon and the creation of an outgoing photon. For low intensities the elastic process dominates such that the outgoing photon has the same frequency and a fixed phase relationship with the incoming one [6,7]. Interferences in this regime have been observed in a seminal experiment by Wineland and co-workers involving two mercury atoms trapped in an ion trap and only weakly excited by a near-resonant laser [8] (see also Refs. [9–14]).

However, when increasing the intensity of the laser, the atomic emitters undergo internal dynamics which may alter the emitted photon frequency and phase. Such inelastic scattering processes lead to a reduced mutual coherence of the light fields, i.e., the emission of partially coherent light, resulting in a decrease of the visibility of the interference fringes [13]. In the case of a very intense driving laser, the atoms emit fully incoherent fluorescence light [15]; in this case the visibility of the fringe pattern disappears.

Aside from the internal dynamics, the driving laser affects additionally the external degrees of freedom of the ions as the laser is used likewise for laser cooling of the particles. The ion temperature plays an important role for the fringe visibility as it determines the localization of the scatterers, i.e., of the slits. Since an increased laser intensity alters both the ratio of elastic to inelastic scattering as well as the localization of the atoms, the influence of inelastic scattering on the mutual coherence of the scattered light has not been observed experimentally.

In this Letter we study the visibility of Young interference fringes produced by individual atoms employing a gated detection method to clearly separate the effect of inelastic scattering from that of reduced atom localization. A theoretical model to explain the measured fringe patterns is developed, taking into account the multilevel structure of the atoms and the presence of a repumping laser. Experimentally, we investigate ion crystals with up to four ions in a harmonic trap potential or in specially shaped trapping fields that allow for the adjustment of the interatomic distances. In this way we are able to form linear arrays of ions serving as a regular grating of atomic scatterers.

For the experiments we employ $^{40}Ca^{+}$ ions trapped in a segmented Paul trap [16]. With trap frequencies $\omega_{r_1,r_2,z}/(2\pi) = (1.853, 2.620, 0.977)$ MHz the ions form linear crystals that align along the weakest trap axis $\mathbf{e}_z$. The electric dipole transition $4^2S_{1/2} \rightarrow 4^2P_{1/2}$ of $^{40}Ca^{+}$ near 397 nm is used for Doppler cooling and light scattering. The $4^2P_{1/2}$ state decays with a probability of 7% to the metastable $3^2D_{3/2}$ level [17]; therefore, we use a laser near 866 nm for repumping to maintain continuous Doppler cooling [see Fig. 1(a)]. The radial modes ω_{r_1,r_2} are aligned along the $\mathbf{e}_{\pm x+y}$ direction, respectively, whereas the cooling and repumping laser illuminate the ion crystals along the $(x, y, z) = (\pm 1, 0, -1)/\sqrt{2}$ direction, respectively, so that the $\mathbf{k}$-vectors of the laser beams have a projection on all vibrational axes of the ion crystal [see Fig. 1(b)].

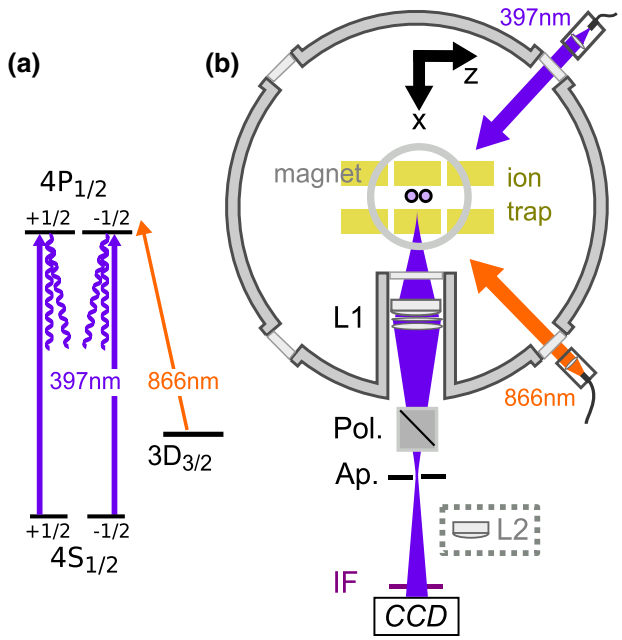

FIG. 1. (a) Level scheme and relevant transitions of the $^{40}Ca^{+}$ ion including the metastable $3^2D_{3/2}$ state. (b) Sketch of experimental setup: Ions are held in a segmented microtrap (yellow), forming linear crystals along the z axis, and are illuminated by laser light near 397 and 866 nm (for details see text).

A magnetic field of ~0.24 mT oriented along $\mathbf{e}_y$, generated by a permanent magnet ring placed on top of the vacuum chamber, determines the quantization axis. The laser beam near 397 nm, having a waist of about 600 μm at the ions' positions, is linearly polarized along this axis and thus excites the $\Delta m = 0$ transitions [see Fig. 1(a)]. The light scattered by the ions is collected by a $f/1.6$ objective $L1$ (focal length 67 mm) at a working distance of 48.5 mm and focused at a distance of about 770 mm, after being sent through a polarization beam splitter (Pol.) oriented along $\mathbf{e}_y$, i.e., the same axis as the cooling laser [see Fig. 1(b)]. An aperture (Ap.) (diameter ~400 μm) is placed at the back focal plane of the objective suppressing unwanted stray light in combination with an infrared filter [(IF), center wavelength $\lambda = 394 \pm 10$ nm]. The scattered light is finally recorded by a CCD camera positioned ~100 mm behind the back focal plane of the objective to observe the light in the far field, i.e., the Fourier plane of the ions. We use either an electron multiplier gain intensifier enhanced CCD camera (EMCCD, Andor iXon 860) or, alternatively, an intensified CCD camera (ICCD, Andor iStar 334T) with 128×128 pixels (pixel size 24.5 μm) and 1024×1024 pixels (pixel size 13 μm), respectively. A lens L2 (focal length $f = 25$ mm), optionally placed in the scattered light beam behind the aperture, focuses the back focal plane onto the CCD, allowing one to image and observe the ions individually, e.g., to check for the number of ions, to determine the magnification of the optical system, or to adjust the axial potential.

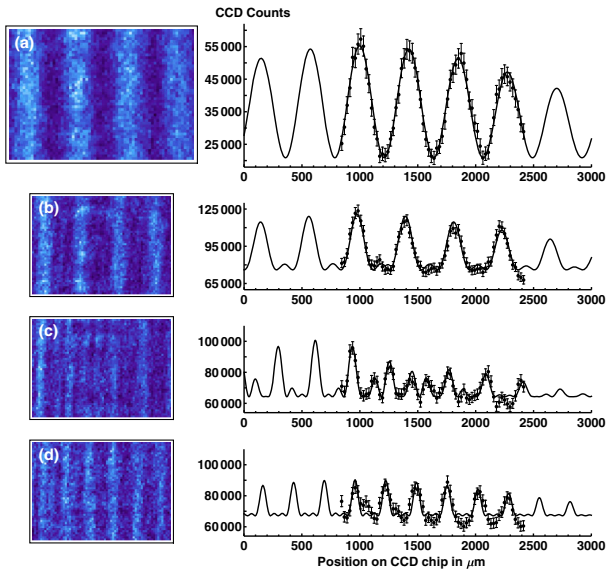

FIG. 2. Images of the EMCCD camera (left) and interference fringe patterns (right) for (a) two, (b) three, and (c) four ions in a harmonic trap potential. In (d) data are presented for a crystal with four equidistant ions. The EMCCD images have been rotated, distortion corrected, and the background has been subtracted (for details see text). Note that the data of the EMCCD camera include the internal avalanche gain and are integrated over an exposure time of 60 s. The fringe patterns are obtained from the corrected EMCCD images by integration over the vertical axis. Errors on each data point correspond to photon shot noise, dark noise, and read-out noise. From a fit of the experimental curves we obtain a visibility $\mathcal{V}$ of the fringe patterns of 45.2(6)%, 22.7(6)%, 22(1)%, and 15(1)% for the two-, three-, and four-ion crystal, and the equidistant four-ion array, respectively, where the errors represent the rms deviation of each fit.

The results of the interference measurements for two, three, and four ions are shown in Fig. 2. The inner parts of the CCD images (68×48 pixels) are rotated and corrected for field distortions measured independently by observing the distance of a two-ion crystal at different positions within the field of view of the CCD. Remaining stray light and background are subtracted from the CCD images, determined by shutting off the repumping laser. The fringe patterns at the right-hand side of Fig. 2 are obtained from the CCD images by integration over the vertical axis; the error bars of ~5% are deduced from photon shot noise. The fits to the interference patterns are derived from the source distribution via Fourier transformation, taking into account the resolution of the imaging device. From the fit parameters we determine the distance d between the ions, the width w of the point spread function (PSF), and the visibility $\mathcal{V}$ of the interference fringes. From Fig. 2(a), we obtain a distance $d = 6.4$ μm and a width of the PSF $w = 3.6$ μm for the two-ion crystal. Note that the calculated magnification of the optical system—derived from the image of the back focal plane of $L1$ on the CCD by use of $L2$—depends on the exact x position of $L2$, which can be

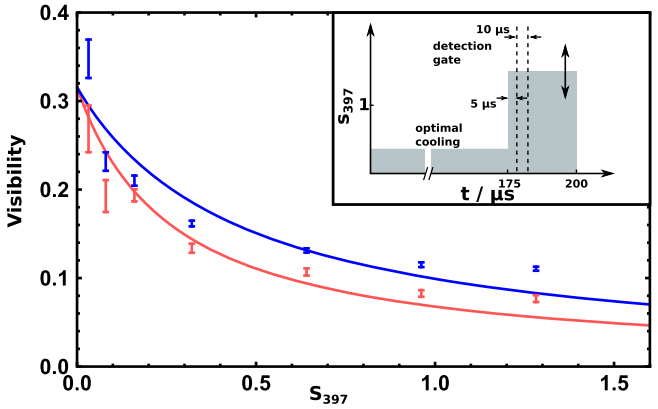

FIG. 3. Interference fringe visibility at the crossover of elastic to inelastic scattering for a two-ion crystal as a function of laser saturation s_{397}. The repumping laser saturation corresponds to $s_{866} = 0.032$ (red dots) and $s_{866} = 0.15$ (blue squares). As in Fig. 2 vertical error bars represent the root mean square deviation of each fit. Note that the data have been obtained after the setup was modified to allow for the GCPD technique. Thus several experimental parameters are not exactly equal to Fig. 2, including a possible misalignment of the quantization axis. The conversion from the measured laser powers into saturation involves the knowledge of the laser waists $\emptyset_{397} = 600(\pm 300)$ μm, $\emptyset_{866} = 300(\pm 150)$ μm and laser detunings $\Delta_{397} = -10$ MHz, $\Delta_{866} = +60(\pm 10)$ MHz. All listed uncertainties lead to a systematic uncertainty of s_{397} of about 100%.

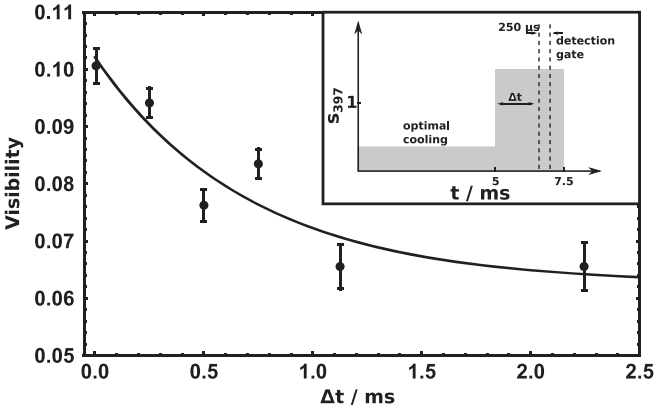

FIG. 4. Dynamical change of the interference fringe visibility $\mathcal{V}$ when heating up the two-ion crystal (for details and explanation of the inset see text).

positioned with an accuracy of ~2 mm. In view of this uncertainty we see good agreement of the determined value d with the independently deduced $d_{\text{theo.}} = 5.8$ μm, based on (i) a spectroscopic determination of the COM-mode frequency of the crystal and (ii) the calculation according to Ref. [18].

Key for the further studies is the gated cooling probe detection (GCPD) of the scattered photons made possible by our intensifier enhanced CCD camera. The GCPD scheme works as follows (see Fig. 3): The ion crystals are initialized during 175 μs via Doppler cooling under optimum conditions for the saturation s_{397} and s_{866} of the cooling and repumping lasers at 397 and 866 nm, i.e., well below the respective saturation intensities, and with a cooling and repumping laser detuning of $\Delta_{397} = -10$ MHz and $\Delta_{866} = +60$ MHz, respectively. We choose the laser detuning for the laser at 866 nm to the blue side of the resonance in order to avoid complications from dark resonances. Thereafter, the saturation of the cooling laser s_{397} is switched to a different value using an acousto-optical modulator. After a delay of 5 μs to allow for proper switching of the laser, the CCD is gated for 10 μs to observe the scattered light at 397 nm. As the motional states of the ion crystals evolve over much longer time scales (see Fig. 4), they are unable to adapt to the modified cooling laser saturation within this detection time. In this way the mutual coherence of the scattered light fields is solely determined by the internal degrees of freedom of the ions.

We can thus investigate the visibility of the interference pattern as a function of the laser saturation without being affected by the ion temperature.

In the paraxial approximation and for scalar fields, i.e., for identical polarization of excitation and detection, the intensity produced by a two-ion crystal at the CCD is [19]

$$I(\mathbf{r},t) = I_1(\mathbf{r},t) + I_2(\mathbf{r},t) + 2\sqrt{I_1(\mathbf{r},t)}\sqrt{I_2(\mathbf{r},t)}\,\mathrm{Re}\{\gamma(\mathbf{r}_1,\mathbf{r}_2,\tau)\}, \quad (1)$$

where $I_1(\mathbf{r},t)$ $[I_2(\mathbf{r},t)]$ is the intensity at $\mathbf{r}$ if ion 2 (ion 1) is absent, $\mathrm{Re}\{.\}$ denotes the real part and $\varphi = kc\tau = k(|\mathbf{r}-\mathbf{r}_1| - |\mathbf{r}-\mathbf{r}_2|)$ is the relative phase accumulated by the fields at $\mathbf{r}$. In Eq. (1), $\gamma(\mathbf{r}_1,\mathbf{r}_2,\tau) = \langle E_1(\mathbf{r}_1,t-\tau)E_2^*(\mathbf{r}_2,t)\rangle / \sqrt{\langle|E_1(\mathbf{r}_1)|^2\rangle\langle|E_2(\mathbf{r}_2)|^2\rangle}$ corresponds to the complex degree of coherence that describes the mutual coherence of the two light fields $E_1(\mathbf{r}_1,t)$ and $E_2(\mathbf{r}_2,t)$, generated by ion 1 at $\mathbf{r}_1$ and ion 2 at $\mathbf{r}_2$, respectively. We assume identical excitation strength and thus equal intensities $I_1(\mathbf{r},t) = I_2(\mathbf{r},t) \equiv I_0$ of the two ions. The visibility of the interference fringes is then equal to the modulus of the complex degree of coherence and the fringe modulation determined by the phase φ.

In a three-level model and with the ions at fixed positions, the intensity distribution on the CCD is (see Supplemental Material [20])

$$I(\mathbf{r}) = 2I_0(1 + |\rho_{sp}|^2/\rho_{pp}\cos\varphi), \quad (2)$$

where ρ_{sp} denotes the single atom coherence between states $s = S_{1/2}$ and $p = P_{1/2}$, and ρ_{pp} is the population of the excited state decaying either to s or level $d = D_{3/2}$. According to Eq. (2) the visibility of the interference pattern is given by

$$\mathcal{V} = |\gamma| = |\rho_{sp}|^2/\rho_{pp}. \quad (3)$$

A reduction of $\mathcal{V}$ is thus predicted for growing ρ_{pp} and reduced ρ_{sp}. If we model the ions as two-level atoms

[for which Eqs. (2) and (3) equally hold] this occurs for increased laser saturation s_{397}. However, the two-level model does not take into account the modification of ρ_{sp} and ρ_{pp} due to the additional decay channel to d. In this case ρ_{sp} and ρ_{pp}, and thus Eq. (3), become more involved functions of the laser parameters.

The measured $\mathcal{V}$ produced by two-ion crystals as a function of s_{397} is shown in Fig. 3. A reduction of $\mathcal{V}$, corresponding to the emission of partially coherent light, is observed when increasing s_{397}, which agrees well with the two-level model. When the saturation of the repumping laser is increased by a factor of ~4 we observe, however, an increased visibility. This behavior is well described by the three-level model fit curves in Fig. 3 (see Supplemental Material [20]).

The visibilities displayed in Fig. 3 are limited by a constant prefactor of ~0.3. Assuming this factor is only due to the motional excitation of the ion crystal results in a mean wave packet size (rms of breathing and rocking modes) of 96(5) nm [9]. This is, however, about a factor 2.3 larger than that expected for the Doppler cooling limit, calculated for the given trap frequencies and unsaturated cooling; indeed, we measured a mean wave packet size of 42(11) nm using sideband spectroscopy [23]. We suspect, therefore, that the prefactor is also affected by misalignment of the quantization axis.

The GCPD scheme can also be employed to investigate the modification of the fringe visibility due to vibrational excitations of the ion crystal. Again, we initialize the crystal by Doppler cooling under optimum conditions ($s_{397} \sim 0.25$, $s_{866} \sim 0.16$). The laser saturation s_{397} is then rapidly increased by a factor of ~5 while keeping the detuning unchanged. Here the CCD is gated to observe the scattered photons in a time interval of 250 μs while we shift the beginning of this time interval from $\Delta t = 0$ to 2.5 ms (see inset of Fig. 4). As the crystal is exposed to a higher saturation, the Doppler cooling limit and the mean phonon number in the breathing and rocking modes increases [8]. The visibility of the fringe pattern is proportional to the Debye Waller factor $\exp\{-\frac{1}{2}\langle[\mathbf{k}_{\mathrm{eff}} \cdot (\mathbf{u}_1 - \mathbf{u}_2)]^2\rangle\}$, where $\mathbf{u}_i$ denotes the fluctuation about the equilibrium positions of ion $i = 1, 2$, $\mathbf{k}_{\mathrm{eff}}$ is the k-vector difference of the absorbed and emitted photons, and $\langle\rangle$ denotes the average over the thermal distributions [9].

In the experiment, the decrease of the fringe visibility as a function of Δt is clearly visible (see Fig. 4), following an exponential decay with a time constant $\tau = 0.7(4)$ ms. The long time constant confirms our assumption that the time evolution of internal and external degrees of freedom of the ions can be separated by use of the GCPD approach. We have obtained similar data for the increase of $\mathcal{V}$ when an initially higher crystal temperature is reduced by Doppler cooling.

Modern trap technology [24,25], where the dc trap potential is shaped by multiple control segments, allows one to modify the trap potential along $\mathbf{e}_z$ and thus the interion distances. This becomes particularly relevant for crystals with ≥ 4 ions. If a crystal with four ions is kept in a harmonic trap, the equilibrium positions of the ions are nonequidistant [18], e.g., for trap frequencies $\omega_{r_1,r_2,z}/(2\pi) = (1.978, 2.180, 0.429)$ MHz the distance between the innermost ions is 7.2 μm and between the outer and the inner ions 7.6 μm, respectively. This results in an interference fringe signal with two spatial frequencies [see Fig. 2(c)]. By adjusting the trap control electrode voltages we are able to generate a nonharmonic potential [26] such that a regular crystal with equal ion separation of 9.1 μm is obtained [see Fig. 2(d)]. The corresponding fringe pattern matches the intensity distribution of a coherently illuminated four-slit grating.

In conclusion, we studied the mutual coherence of light fields emitted by individual atoms at the crossover from elastic to inelastic scattering. We implemented a detection scheme allowing us to observe the degree of mutual coherence as a function of the saturation of the observed $S_{1/2} \rightarrow P_{1/2}$ transition at fixed ion crystal temperatures. The decrease of the visibility of the interference patterns due to motional effects of the ions was investigated separately. The method could pave the way towards temperature measurements of ion crystals at low trap frequencies where standard sideband methods, highly successful in tightly confining potentials [23], become increasingly hard. We also see applications when the trap potential is adiabatically lowered [27], e.g., when ions are loaded into optical potentials [28–30]. The experiment also provides opportunities to investigate multi-ion entanglement [31–36] or measurements of photon-photon correlations and their backaction on the ion crystals [37–39].

We gratefully acknowledge the support of LOT-QuantumDesign for lending the ICCD. We thank S. T. Dawkins for carefully reading the text. F. S. K. and S. W. acknowledge the financial support of the Cluster of excellence PRISMA at the Johannes-Gutenberg Universität Mainz and the DFG within the project BESCOOL. J. vZ gratefully acknowledges funding by the Erlangen Graduate School in Advanced Optical Technologies (SAOT) by the German Research Foundation (DFG) in the framework of the German excellence initiative.

*wolfs@uni-mainz.de
†http://www.quantenbit.de

[1] M. H. Shamos, *Great Experiments in Physics: Firsthand accounts from Galileo to Einstein* (Courier Corporation, North Chelmsford, MA, 1959).
[2] P. A. M. Dirac, *The Principles of Quantum Mechanics* (Oxford Science Publications, New York, 1989).
[3] R. Loudon, *The Quantum Theory of Light* (Oxford University Press, New York, 2000).

[4] C. Cohen-Tannoudji, J. Dupont-Roc, and G. Grynberg, *Photons and Atoms: Introduction to Quantum Electrodynamics* (Wiley-VCH, New York, 2004).

[5] M. O. Scully and M. S. Zubairy, *Quantum Optics* (Cambridge University Press, Cambridge, England, 1997).

[6] J. T. Höffges, H. W. Baldauf, T. Eichler, S. R. Helmfrid, and H. Walther, Heterodyne measurement of the fluorescent radiation of a single trapped ion, Opt. Commun. **133**, 170 (1997).

[7] J. Eschner, C. Raab, F. Schmidt-Kaler, and R. Blatt, Light interference from single atoms and their mirror images, Nature (London) **413**, 495 (2001).

[8] U. Eichmann, J. C. Bergquist, J. J. Bollinger, J. M. Gilligan, W. M. Itano, D. J. Wineland, and M. G. Raizen, Young's interference experiment with light scattered from two atoms, Phys. Rev. Lett. **70**, 2359 (1993).

[9] W. M. Itano, J. C. Bergquist, J. J. Bollinger, D. J. Wineland, U. Eichmann, and M. G. Raizen, Complementarity and Young's interference fringes from two atoms, Phys. Rev. A **57**, 4176 (1998).

[10] Z. Ficek and S. Swain, *Quantum Interference and Coherence: Theory and Experiments* (Springer Science & Business Media, New York, 2005), Vol. 100.

[11] R. G. DeVoe and R. G. Brewer, Observation of Superradiant and Subradiant Spontaneous Emission of Two Trapped Ions, Phys. Rev. Lett. **76**, 2049 (1996).

[12] T. Wong, S. M. Tan, M. J. Collett, and D. F. Walls, Interference of resonance fluorescence from two four-level atoms, Phys. Rev. A **55**, 1288 (1997).

[13] C. Skornia, J. von Zanthier, G. S. Agarwal, E. Werner, and H. Walther, Nonclassical interference effects in the radiation from coherently driven uncorrelated atoms, Phys. Rev. A **64**, 063801 (2001).

[14] C. Schön and A. Beige, Analysis of a two-atom double-slit experiment based on environment-induced measurements, Phys. Rev. A **64**, 023806 (2001).

[15] B. R. Mollow, Power Spectrum of Light Scattered by Two-Level Systems, Phys. Rev. **188**, 1969 (1969).

[16] G. Jacob, K. Groot-Berning, S. Wolf, S. Ulm, L. Couturier, S. T. Dawkins, U. G. Poschinger, F. Schmidt-Kaler, and K. Singer, Microscopy with a Deterministic Single Ion Source, arXiv:1512.00347.

[17] M. Hettrich, T. Ruster, H. Kaufmann, C. F. Roos, C. T. Schmiegelow, F. Schmidt-Kaler, and U. G. Poschinger, Measurement of Dipole Matrix Elements with a Single Trapped Ion, Phys. Rev. Lett. **115**, 143003 (2015).

[18] D. F. James, Quantum dynamics of cold trapped ions with application to quantum computation, Appl. Phys. B **66**, 181 (1998).

[19] L. Mandel and E. Wolf, *Optical Coherence and Quantum Optics* (Cambridge University Press, Cambridge, England, 1995).

[20] See Supplemental Material at http://link.aps.org/supplemental/10.1103/PhysRevLett.116.183002, which includes Refs. [21,22].

[21] C. Cohen-Tannoudji, J. Dupont-Roc, and G. Grynberg, *Atom-Photon Interactions: Basic Processes and Applications* (Wiley-VCH, New York, 1998).

[22] G. S. Agarwal, *Quantum Optics* (Cambridge University Press, Cambridge, England, 2013).

[23] H. Häffner, C. Roos, and R. Blatt, Quantum computing with trapped ions, Phys. Rep. **469**, 155 (2008).

[24] M. Brownnutt, M. Harlander, W. Hänsel, and R. Blatt, Spatially-resolved potential measurement with ion crystals, Appl. Phys. B **107**, 1125 (2012).

[25] J. Home, D. Hanneke, J. Jost, J. Amini, D. Leibfried, and D. Wineland, Complete Methods Set for Scalable Ion Trap Quantum Information Processing, Science **325**, 1227 (2009).

[26] T. Ruster, C. Warschburger, H. Kaufmann, C. T. Schmiegelow, A. Walther, M. Hettrich, A. Pfister, V. Kaushal, F. Schmidt-Kaler, and U. G. Poschinger, Experimental realization of fast ion separation in segmented Paul traps, Phys. Rev. A **90**, 033410 (2014).

[27] G. Poulsen, Y. Miroshnychenko, and M. Drewsen, Efficient ground-state cooling of an ion in a large room-temperature linear Paul trap with a sub-Hertz heating rate, Phys. Rev. A **86**, 051402 (2012).

[28] C. Schneider, M. Enderlein, T. Huber, and T. Schätz, Optical trapping of an ion, Nat. Photonics **4**, 772 (2010).

[29] C. T. Schmiegelow, H. Kaufmann, T. Ruster, J. Schulz, V. Kaushal, M. Hettrich, F. Schmidt-Kaler, and U. G. Poschinger, Phase-Stable Free-Space Optical Lattices for Trapped Ions, Phys. Rev. Lett. **116**, 033002 (2016).

[30] R. Linnet, I. Leroux, A. Dantan, and M. Drewsen, Sub-micron positioning of trapped ions with respect to the absolute center of a standing-wave cavity field, Appl. Phys. B **114**, 295 (2014).

[31] C. Thiel, J. von Zanthier, T. Bastin, E. Solano, and G. S. Agarwal, Generation of Symmetric Dicke States of Remote Qubits with Linear Optics, Phys. Rev. Lett. **99**, 193602 (2007).

[32] T. Bastin, C. Thiel, J. von Zanthier, L. Lamata, E. Solano, and G. S. Agarwal, Operational Determination of Multiqubit Entanglement Classes via Tuning of Local Operations, Phys. Rev. Lett. **102**, 053601 (2009).

[33] D. L. Moehring, P. Maunz, S. Olmschenk, K. C. Younge, D. N. Matsukevich, L.-M. Duan, and C. Monroe, Entanglement of single-atom quantum bits at a distance, Nature (London) **449**, 68 (2007).

[34] S. Ritter, C. Nolleke, C. Hahn, A. Reiserer, A. Neuzner, M. Uphoff, M. Mucke, E. Figueroa, J. Bochmann, and G. Rempe, An elementary quantum network of single atoms in optical cavities, Nature (London) **484**, 195 (2012).

[35] J. Hofmann, M. Krug, N. Ortegel, L. Grard, M. Weber, W. Rosenfeld, and H. Weinfurter, Heralded Entanglement Between Widely Separated Atoms, Science **337**, 72 (2012).

[36] H. Bernien, B. Hensen, W. Pfaff, G. Koolstra, M. S. Blok, L. Robledo, T. H. Taminiau, M. Markham, D. J. Twitchen, L. Childress, and R. Hanson, Heralded entanglement between solid-state qubits separated by three metres, Nature (London) **497**, 86 (2013).

[37] S. Oppel, T. Büttner, P. Kok, and J. von Zanthier, Superresolving Multiphoton Interferences with Independent Light Sources, Phys. Rev. Lett. **109**, 233603 (2012).

[38] D. Gatto Monticone, K. Katamadze, P. Traina, E. Moreva, J. Forneris, I. Ruo-Berchera, P. Olivero, I. P. Degiovanni, G. Brida, and M. Genovese, Beating the Abbe Diffraction Limit in Confocal Microscopy via Nonclassical Photon Statistics, Phys. Rev. Lett. **113**, 143602 (2014).

[39] S. Oppel, R. Wiegner, G. S. Agarwal, and J. von Zanthier, Directional Superradiant Emission from Statistically Independent Incoherent Nonclassical and Classical Sources, Phys. Rev. Lett. **113**, 263606 (2014).